






RESEARCH ARTICLE | SEPTEMBER 22 2020

Phase-field simulation of two-dimensional topological charges in nematic liquid crystals

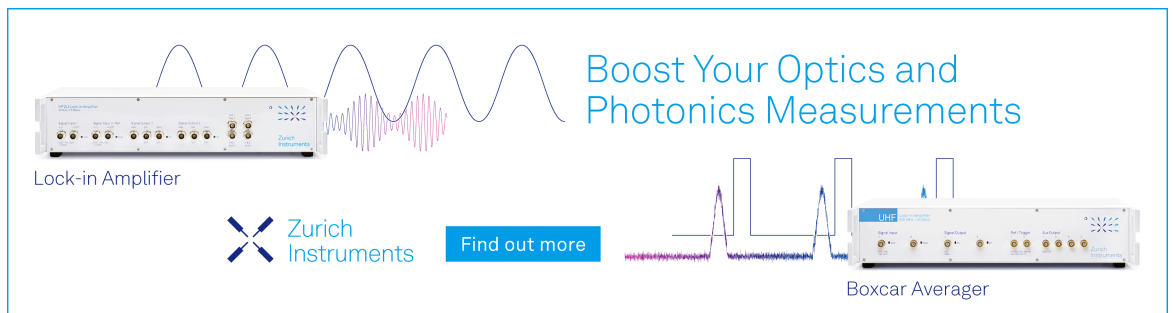
Special Collection: [Advances in Processing and Structural Characterization of Complex Soft Matter](#)

Deshan Liang ; Xingqiao Ma  ; Zhuhong Liu ; Hasnain Mehdi Jafri; Guoping Cao; Houbing Huang ; Sanqiang Shi; Long-Qing Chen

 Check for updates


J. Appl. Phys. 128, 124701 (2020)

<https://doi.org/10.1063/5.0021079>



Boost Your Optics and Photonics Measurements

Lock-in Amplifier

 Zurich Instruments

[Find out more](#)

Boxcar Averager

Phase-field simulation of two-dimensional topological charges in nematic liquid crystals

Cite as: J. Appl. Phys. 128, 124701 (2020); doi: 10.1063/5.0021079

Submitted: 9 July 2020 · Accepted: 30 August 2020 ·

Published Online: 22 September 2020



Deshan Liang,¹ Xingqiao Ma,^{1,a)} Zhuhong Liu,¹ Hasnain Mehdi Jafri,^{1,2} Guoping Cao,³ Houbing Huang,² Sanqiang Shi,⁴ and Long-Qing Chen⁵

AFFILIATIONS

¹Department of Physics, University of Science and Technology Beijing, Beijing 100083, China

²Advanced Research Institute of Multidisciplinary Science, Beijing Institute of Technology, Beijing 100081, China

³National Center for Electron Microscopy in Beijing, Key Laboratory of Advanced Materials of Ministry of Education of China and State Key Laboratory of New Ceramics and Fine Processing, School of Materials Science and Engineering, Tsinghua University, Beijing 100084, China

⁴Department of Mechanical Engineering, The Hong Kong Polytechnic University, Hung Hom, Kowloon, Hong Kong

⁵Department of Materials Science and Engineering, The Pennsylvania State University, University Park, Pennsylvania 16802, USA

^{a)}Author to whom correspondence should be addressed: xqma@sas.ustb.edu.cn

ABSTRACT

The concept of topological quantum number, or topological charge, has been used extensively to describe topological defects or solitons. Nematic liquid crystals contain both integer and half-integer topological defects, making them useful models for testing the rules that govern topological defects. Here, we investigated topological defects in nematic liquid crystals using the phase-field method. If there are no defects along a loop path, the total charge number is described by an encircled loop integral. We found that the total charge number is conserved, and the conservation of defects number is determined by a boundary during the generation and annihilation of positive-negative topological defects when the loop integral is confined. These rules can be extended to other two-dimensional systems with topological defects.

Published under license by AIP Publishing. <https://doi.org/10.1063/5.0021079>

INTRODUCTION

The defects in liquid crystals can be described in some cases by topological charges. The topological charge is one of the most widely used topological concepts in physics. A topological charge of defect is a spatial point around which the loop integral¹ $q = 1/2\pi \oint d\theta$, where $d\theta$ is the angle difference between the directions of the field at the beginning and ending points of a small segment, dl , of the loop [Fig. 1(a)]. Topological charge of defects usually have either integer or half-integer values and may be positive or negative, depending on the nature of the corresponding physical fields. Therefore, topological defects can be regarded as quasi-particles; they can move, interact, generate, and annihilate.² Treating topological defects as particles, rather than describing them in terms of fields, typically simplifies the corresponding model.

The concept of topological defects charge has been applied to many systems, including systems that exhibit quantum Hall

effects,³ vortex systems in superconductors,⁴ handle body-shaped particles,^{5–7} surface-treated microparticles,^{8,9} micrometer-sized beads,¹⁰ optical and electrical reversible switching,¹¹ epithelial cells,¹² and fibers dipped in liquid crystals (LCs).¹³ The topological charge has also been applied to active matter,^{14–17} cosmology,¹⁸ and particle physics.¹⁹ The relationships between the genus g , the topological charge of defects, and self-assembly²⁰ have been found to be consistent between the systems in which they have been characterized.

Nematic liquid crystal (NLC) molecules have a rod-like shape. The physical properties of a non-polarized NLC are the same at either end. For a closed loop formed by NLC molecules, the director revolves by times of 180° in a nonpolar NLC; this process may generate half-integer topological defects. In a polarized NLC, the loop repeats every 360° , which may result in the generation of integer topological defects. Therefore, NLC systems contain both

17 May 2024 08:34:38

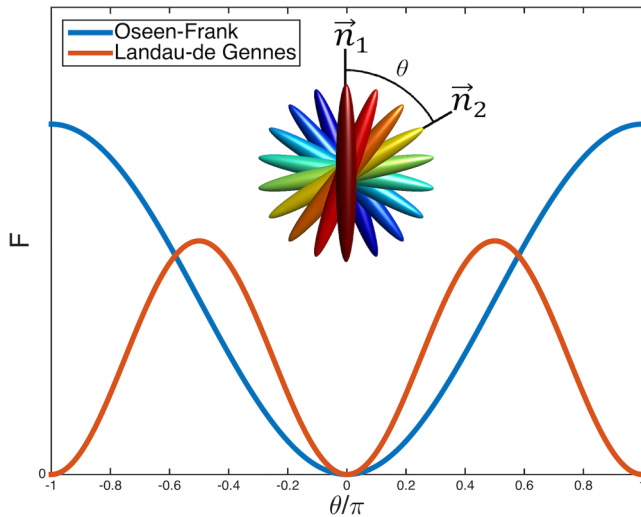


FIG. 2. Diagram of energy density vs director angle. The inset shows an illustration of the director angle θ .

where Γ is the viscosity coefficient of NLCs. Numerical solutions to Eq. (10) yield the spatial and temporal distributions of NLC directors and, therefore, the domain and defect evolution in NLCs.

We defined a new field $\vec{\mathfrak{B}} = (\vec{n} \times \partial_x \vec{n} \cdot \vec{N}, \vec{n} \times \partial_y \vec{n} \cdot \vec{N}, \vec{n} \times \partial_z \vec{n} \cdot \vec{N})$, where \vec{n} is the director, \vec{N} is the unit vector along the plane normal [Fig. 1(a)], and $\partial_x \vec{n}$ is the rate of change of \vec{n} in the x direction. The value of $\vec{n} \times \partial_x \vec{n} \cdot \vec{N}$ is equal to the angle change of \vec{n} in the x direction.

In Fig. 2, red and blue lines correspond to the L-dG and O-F energy models, respectively, k_{11} , k_{22} , and k_{33} are assumed to be equal, and θ is the angle between \vec{n}_1 and \vec{n}_2 (Fig. 2, inset).

In NLCs, $-\vec{n}$ is generally equivalent to \vec{n} , because non-polarized NLC molecules are indistinguishable. Therefore, $\theta = \pm\pi$ and $f(\pi) = f(-\pi) = f(0)$. The L-dG model has been shown to be more consistent with the actual symmetry of NLCs than the O-F model. However, the O-F model has a simpler expression for the free energy than the L-dG model and comparable accuracy in systems with integer charge topological defects. Therefore, the O-F model can be used to simplify NLC models that exclude half-integer defects and to simulate hybrid aligned nematic, optically compensated bend, and twisted nematic LC systems.

RESULTS AND DISCUSSION

Figure 3 shows a schematic diagram of defect energy as a function of charge number (q), calculated using the L-dG and O-F models. In addition, Fig. 3 shows integer (top) and half-integer (bottom) texture maps. The results shown in Fig. 3 demonstrate that, in the O-F model, the half-integer defects are in a high-energy, unstable state and, therefore, will not appear during defect evolution. The L-dG model can be used to describe integer and half-integer topological defects. The following discussion is based on phase-field simulations using the L-dG model.

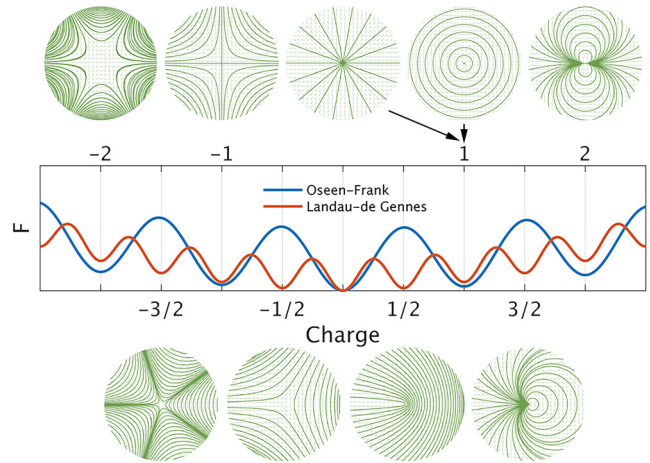


FIG. 3. Comparison between half-integer (bottom) and integer (top) defects. Solid green lines represent the texture, and dotted green lines represent the liquid crystal orientation. The central graph shows energy vs the charge numbers ($q = \frac{1}{2\pi} \oint d\theta$) of defects. Results based on the Landau-de Gennes and Oseen-Frank models are represented by the red and blue lines, respectively.

To determine the relationship between the topological defects and the loop integral, we simulated NLCs assuming a regular area with two holes ($g = 2$) and considered voids and other discontinuities in the system. The distributions of directors and defects are shown in Fig. 4. The red and blue markers in Fig. 4 represent topological defects charge of $q = +1/2$ and $q = -1/2$, respectively. Annihilation of opposite topological charges occurred between the states shown in Figs. 4(a) and 4(b). A single annihilation event occurred from Figs. 4(b) and 4(c).

Figures 4(d)–4(f) show the polarizing optical microscopic (POM) images calculated from the director distribution in Figs. 4(a)–4(c). The boundary conditions along the loop assume that the directors are parallel to the direction of the loop. The results are shown in Figs. 4(a)–4(c) demonstrate that defects evolution obeys pairwise ($+1/2$ and $-1/2$) annihilation within the plane. During these annihilation processes, the sum of the topological defects charge on the plane is conserved. Annihilation between $+1$ and -1 topological defects has been observed experimentally in LCs.² In this study, the annihilation was found to follow the law of charge conservation. Similar topological defects charge conservation phenomena have been observed in rod-like virus bacteriophage systems.³¹

Assume that there is a 2D system with several topological defects. If a loop is drawn that encircles the defects and genera, then the enclosed area may be divided into many smaller areas [Fig. 1(b)]. For a single small area, a loop can be defined along its boundary, for example, counterclockwise. If there is a topological charge q_i within this loop, then $q_i = \frac{1}{2\pi} \oint \vec{\mathfrak{B}} \cdot d\vec{l}$, where the integral is taken along the boundary path of the small area. If there is no topological defect within this small area, then $q_i = 0$. For two adjacent small areas, the loop integrals contain a common segment \overline{ab} , wherein the directions of the integrals of the neighboring loops are

17 May 2024 08:34:38

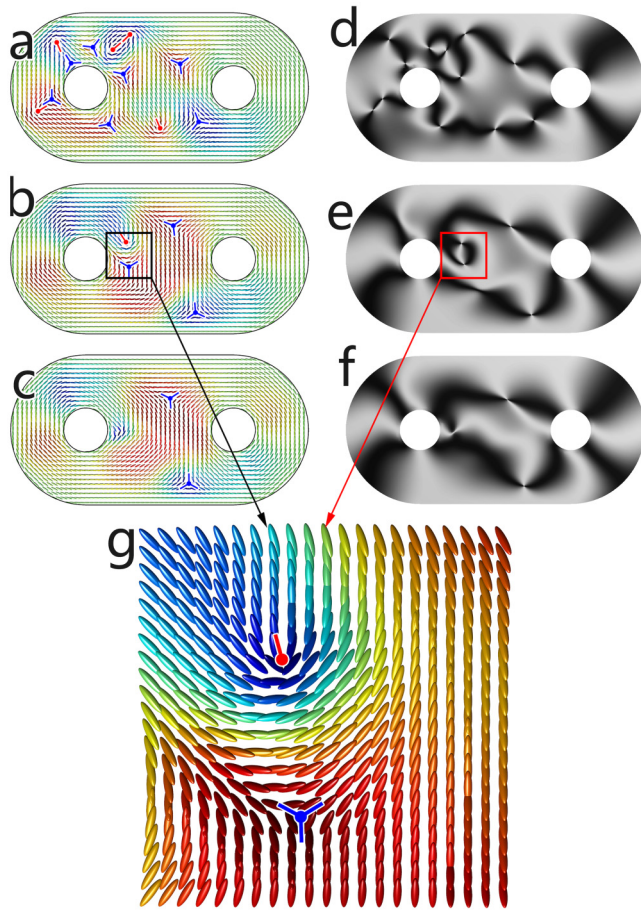


FIG. 4. Directors and defect charge distributions in NLC systems. (a)–(c) are the director distributions at $t = (75k, 120k, 141k)\Delta t$. (g) is a magnified region of (c), showing a pair of defects with charges of $q = +1/2$ and $q = -1/2$, represented by red and blue markers, respectively. (d)–(f) are polarizing optical microscopy (POM) images calculated from (a)–(c), respectively. The gradient color indicates the extent to which the liquid crystal director is tilted out of the plane.

opposed. When the loop integrals of these neighboring areas are added together, the two integrals cancel out within \overline{ab} . Hence, the common segment of adjacent areas does not contribute to the sum of the integrals. Because the internal segments are all common segments between adjacent areas, their contributions to the total sum are zero. When the loop integrals of the small areas are added together, only the integrals along the boundary path of the large area contribute to the final result. Moreover, if both the inner and outer boundary paths proceed counterclockwise, then we have the following equation:

$$\sum_i q_i = \frac{1}{2\pi} \oint_{l-out} \vec{\mathfrak{B}} \cdot d\vec{l} - \frac{1}{2\pi} \sum \oint_{l-in} \vec{\mathfrak{B}} \cdot d\vec{l}, \quad (14)$$

where $d\vec{l}$ is an infinitesimal vector tangent to the loop path $l-in$ or $l-out$, where $l-in$ and $l-out$ represent the inside and outside boundaries, respectively. In Fig. 1(a), \vec{l}_u is a unit vector tangent to l . Because the director field is continuous, the terms on the right side of Eq. (14) are either integers or half-integers.

In a simply connected domain, that is, if there is no inside boundary ($l-in$), Eq. (14) can be simplified as follows:

$$\sum_i q_i = \frac{1}{2\pi} \oint_{l-out} \vec{\mathfrak{B}} \cdot d\vec{l}, \quad (15)$$

where

$$\oint_{l-out} \vec{\mathfrak{B}} \cdot d\vec{l} = 2\pi \sum_i q_i, \quad (16)$$

$$\oint_{l-out} \vec{B} \cdot d\vec{l} = \mu_0 \sum_i I_i, \quad (17)$$

where \vec{B} is the magnetic field at a closed loop. $l-out$ is an Ampèrian loop, and I_i is the stationary electric current enclosed by the loop. Equations (16) and (17) have similar forms. We newly defined field “ \mathfrak{B} ” which is similar to the magnetic field B in the Ampere’s circuital law. On the right side of Eq. (16), coefficient 2π

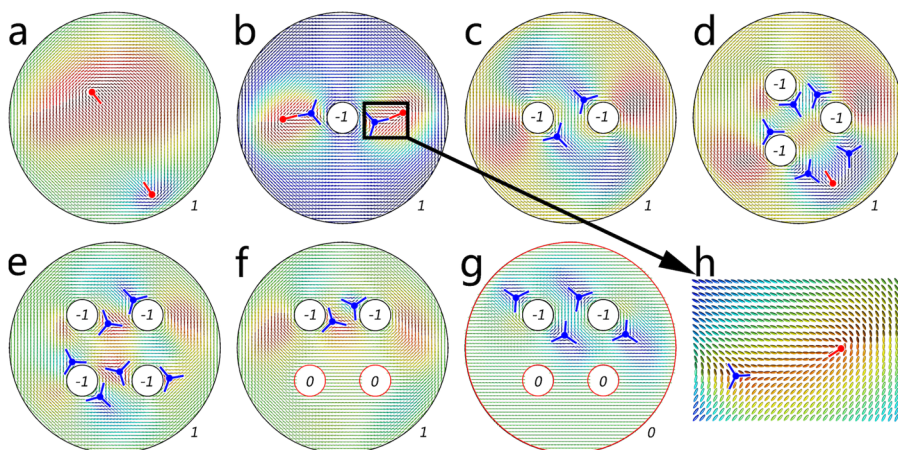


FIG. 5. Director distributions of NLCs of different shapes or under different boundary conditions. (a)–(g) show the simulation results from the L-dG model. Red and blue markers represent $+1/2$ defects and $-1/2$ defects, respectively. The number at the bottom right corner of each image is V_{out} . The number of genera in each image is V_{in} . (e)–(g) have the same numbers of genera and the same Euler–Poincaré characteristics. Black boundary lines indicate that the direction of the directors at the boundary is parallel to the boundary line. Red boundary lines indicate that directors at the boundary are not parallel to the boundary line. (h) shows a magnified section of (b).

17 May 2024 08:34:38

TABLE I. Defect charges resulting from genus and boundary conditions. g is the genus, χ is the Euler–Poincaré characteristic, $V_{out} = \frac{1}{2\pi} \oint_{\mathcal{J}_{l-out}} \vec{\mathfrak{B}} \cdot d\vec{l}$, $V_{in} = -\frac{1}{2\pi} \oint_{\mathcal{J}_{l-in}} \vec{\mathfrak{B}} \cdot d\vec{l}$, and q is the topological charge.

g	χ	V_{out}	V_{in}	$q = +1/2$	$q = -1/2$	$\sum_i q$	$V_{out} + V_{in}$	Figure	Line No.
0	1	1	0	2	0	1	1	5(a)	1
1	0	1	-1	2	2	0	0	5(b)	2
2	-1	1	-2	0	2	-1	-1	5(c)	3
3	-2	1	-3	1	5	-2	-2	5(d)	4
4	-3	1	-4	0	6	-3	-3	5(e)	5
4	-3	1	-2	0	2	-1	-1	5(f)	6
4	-3	0	-2	0	4	-2	-2	5(g)	7

corresponds to the magnetic permeability μ_0 , and the charge of topological defects q_i corresponds to the current I_i . Because the general proof of Eq. (14) is unrelated to NLCs, this is a very general result and may be extended to topological systems other than rod-like NLCs.

To validate Eq. (14), we performed phase-field simulations of NLCs with different genus numbers using a system containing $128 \times 128 \times 4$ mesh points, with a grid size of $10 \mu\text{m}$. Figure 5 shows the director distributions from the phase-field simulations. Each distribution corresponds to a different row in Table I. In Figs. 5(a)–5(e), the orientations of the NLC molecules are parallel to the inner and outer boundary lines. In Fig. 5(f), the orientations of the molecules at the boundary of the two lower genera are horizontal and are not parallel to the boundary of the genus. We numerically calculated the integral of the field $\vec{\mathfrak{B}}$ along the loop around the outer boundary of the studied area and the inner boundaries of the genera. Hence, we observed that $V_{out} = \frac{1}{2\pi} \oint_{\mathcal{J}_{l-out}} \vec{\mathfrak{B}} \cdot d\vec{l}$ and $V_{in} = -\frac{1}{2\pi} \oint_{\mathcal{J}_{l-in}} \vec{\mathfrak{B}} \cdot d\vec{l}$ were determined by the outer and inner boundary conditions, respectively.

The boundary conditions are summarized in Table I. Within each row, the sum of the numbers in columns 3 and 4 is equal to the value in column 7 (same as column 8). Thus, $V_{out} + V_{in} = \sum_i q_i$. This demonstrates that the evolution of topological defects charge obeys charge conservation and that the sum of topological defects charge is determined by the loop integrals along the loop boundaries. The topological theory defines the following relationship: $\chi = 1 - g$, where χ is the Euler characteristic and g is the genus. In the first four cases shown in Table I, the values in columns 2 and 7 are equal, and $\sum_i q = \chi = 1 - g$ holds true. However, $\sum_i q = 1 - g$ does not hold in all cases. For example, the systems shown in Figs. 5(e)–5(g) have the same genus and Euler characteristics but have different $\sum_i q$ values. However, Eq. (14) is unconditionally valid for all of the cases described herein.

CONCLUSIONS

In summary, the total topological defects charge number within an arbitrarily selected enclosed loop obeys a 2D topological circuital charge law described by the following equation: $\sum_i q_i = \frac{1}{2\pi} \oint_{\mathcal{J}_{l-out}} \vec{\mathfrak{B}} \cdot d\vec{l} - \frac{1}{2\pi} \oint_{\mathcal{J}_{l-in}} \vec{\mathfrak{B}} \cdot d\vec{l}$. This law is analogous to the Ampère’s circuital law. In a planar NLC system, the plane boundary has no defects, and the value of the topological defects charge within the plane is determined by the loop integrals along

the boundary paths. If the loop integral is well confined, the defects charge in the loop is conserved. These conclusions may be extended to other 2D systems that contain topological defects charge, such as ferroelectric systems,^{32,33} topological insulators,³⁴ topological superconductors,³⁵ and Majorana fermions.³⁶

ACKNOWLEDGMENTS

This work was supported by grants (Nos. 11174030, 51271157, 11504020, and 51972028) from the National Natural Science Foundation of China (NNSFC).

DATA AVAILABILITY

The data that support the findings of this study are available from the corresponding author upon reasonable request.

REFERENCES

- J. V. Selinger, *Introduction to the Theory of Soft Matter: From Ideal Gases to Liquid Crystals* (Springer, 2015).
- I. Chuang, R. Durrer, N. Turok, and B. Yurke, *Science* **251**, 1336 (1991).
- R. B. Laughlin, *Phys. Rev. Lett.* **50**, 1395 (1983).
- G. Blatter, M. V. Feigel’man, V. B. Geshkenbein, A. I. Larkin, and V. M. Vinokur, *Rev. Mod. Phys.* **66**, 1125 (1994).
- M. G. Campbell, M. Tasinkevych, and I. I. Smalyukh, *Phys. Rev. Lett.* **112**, 197801 (2014).
- B. Senyuk, Q. Liu, S. He, R. D. Kamien, R. B. Kusner, T. C. Lubensky, and I. I. Smalyukh, *Nature* **493**, 200 (2013).
- S. Čopar, *Phys. Rep.* **538**, 1 (2014).
- U. Tkalec and I. Mušević, *Soft Matter* **9**, 8140 (2013).
- T. Araki, F. Serra, and H. Tanaka, *Soft Matter* **9**, 8107 (2013).
- U. Tkalec, M. Ravnik, S. Žumer, and I. Mušević, *Phys. Rev. Lett.* **103**, 127801 (2009).
- I. I. Smalyukh, Y. Lansac, N. A. Clark, and R. P. Trivedi, *Nat. Mater.* **9**, 139 (2010).
- W. Xi, T. B. Saw, D. Delacour, C. T. Lim, and B. Ladoux, *Nat. Rev. Mater.* **4**, 23 (2019).
- E. Terentjev, *Nat. Mater.* **12**, 187 (2013).
- C. H. Peng, T. Turiv, Y. B. Guo, Q. H. Wei, and O. D. Lavrentovich, *Science* **354**, 882 (2016).
- S. J. DeCamp, G. S. Redner, A. Baskaran, M. F. Hagan, and Z. Dogic, *Nat. Mater.* **14**, 1110 (2015).
- L. Giomi, M. J. Bowick, X. Ma, and M. C. Marchetti, *Phys. Rev. Lett.* **110**, 228101 (2013).
- H. R. O. Sohn, C. D. Liu, and I. I. Smalyukh, *Nat. Commun.* **10**, 4744 (2019).
- M. B. Hindmarsh and T. W. B. Kibble, *Rep. Prog. Phys.* **58**, 477 (1995).

- ¹⁹V. Kuzmin, V. Rubakov, and M. Shaposhnikov, *Phys. Lett. B* **155**, 36 (1985).
- ²⁰M. J. Solomon, *Curr. Opin. Colloid Interface Sci.* **16**, 158 (2011).
- ²¹N. D. Mermin, *Rev. Mod. Phys.* **51**, 591 (1979).
- ²²M. Kleman and O. D. Lavrentovich, *Soft Matter Physics: An Introduction* (Springer Science & Business Media, 2007).
- ²³F. C. Frank, *Discuss. Faraday Soc.* **25**, 19 (1958).
- ²⁴G. Di Fratta, J. M. Robbins, V. Slastikov, and A. Zarnescu, *J. Nonlinear Sci.* **26**, 121 (2015).
- ²⁵A. Majumdar and A. Zarnescu, *Arch. Ration. Mech. Anal.* **196**, 227 (2010).
- ²⁶P. De Gennes, J. Prost, E. Olbrich, O. Marinov, and D. Davidov, *Phys. Rev. E* **2713**, 48 (1993).
- ²⁷T. Inukai and K. Miyazawa, *Outline of Development of Nematic Liquid Crystal Compounds for LCD* (The Museum, King's Printer for British Columbia, 1917).
- ²⁸D. W. Berreman and S. Meiboom, *Phys. Rev. A* **30**, 1955 (1984).
- ²⁹L. Longa, D. Monselesan, and H. R. Trebin, *Liq. Cryst.* **2**, 769 (1987).
- ³⁰J. B. Fournier and P. Galatola, *Europhys. Lett. (EPL)* **72**, 403 (2005).
- ³¹O. V. Manyuhina, K. B. Lawlor, M. C. Marchetti, and M. J. Bowick, *Soft Matter* **11**, 6099 (2015).
- ³²S.-Z. Lin, X. Wang, Y. Kamiya, G.-W. Chern, F. Fan, D. Fan, B. Casas, Y. Liu, V. Kiryukhin, W. H. Zurek, C. D. Batista, and S.-W. Cheong, *Nat. Phys.* **10**, 970 (2014).
- ³³F. Xue, X. Wang, I. Socolenco, Y. Gu, L.-Q. Chen, and S.-W. Cheong, *Sci. Rep.* **5**, 17057 (2015).
- ³⁴M. Z. Hasan and C. L. Kane, *Rev. Mod. Phys.* **82**, 3045 (2010).
- ³⁵A. Das, Y. Ronen, Y. Most, Y. Oreg, M. Heiblum, and H. Shtrikman, *Nat. Phys.* **8**, 887 (2012).
- ³⁶L. Fu and C. L. Kane, *Phys. Rev. Lett.* **100**, 096407 (2008).